Available online at www.sciencedirect.com
ScienceDirect
Journal of the European Ceramic Society 30 (2010) 2239–2251
www.elsevier.com/locate/jeurceramsoc

Material property requirements for analysis and design of UHTC components in hypersonic applications

Thomas H. Squire [a], Jochen Marschall [b,*]

[a] NASA Ames Research Center, MS-234, Moffett Field, CA 94035, United States
[b] SRI International, 333 Ravenswood Avenue, Menlo Park, CA 94025, United States

Available online 19 February 2010

Abstract

Analytical modeling of thermal and mechanical response is a fundamental step in the design process for ultra-high-temperature ceramic components, such as nose tips and wing leading edges for hypersonic applications. The purpose of the analyses is to understand the response of test articles to high-enthalpy flows in ground tests and to predict component performance in particular flight environments. Performing these analyses and evaluating the results require comprehensive and accurate physical, thermal, and mechanical properties. In this paper, we explain the nature of the analyses, highlight the essential material properties that are required and why they are important, and describe the impact of property accuracy and uncertainty on the design process.

Keywords: Ultra-high-temperature ceramics; Borides; Mechanical properties; Thermal properties

1. Introduction

Certain characteristics of ultra-high-temperature ceramic (UHTC) materials containing transition metal borides and carbides give them a potential advantage over more traditional materials for use in hypersonic applications. In particular, hafnium and zirconium diborides and carbides, as well as their oxides, hafnia and zirconia, have extremely high melting points, all in excess of 2500 °C (4530 °F).[1] While HfC and ZrC have higher melting points than HfB_2 and ZrB_2, the diborides have substantially higher thermal conductivities than the carbides.[2,3] This combination of high-temperature capability and high thermal conductivity makes HfB_2 and ZrB_2 particularly attractive for use in sharp wing leading edges (WLEs) and nose tips.[4] In practice, the high-temperature oxidation resistance of pure diboride materials is not sufficient for aerothermal flight environments. The best oxidation performance is found for monolithic materials hot-pressed from mixtures of ceramic powders containing a silica former as a minor component.[5,6] The most common compositions typically contain 10–30 vol.% SiC,[7–12] although other silica formers like $MoSi_2$ and $TaSi_2$ have also been investigated.[13–16]

The design of high-performance hypersonic vehicles generally involves relatively sharp nose tips and WLEs. (An arcjet model of a concept UHTC WLE section is shown in Fig. 1.) While not an achievable design in practice, in the context of supersonic flow theory, a "sharp" leading edge is one with zero radius of curvature. In a practical design context, "sharp" usually refers to a leading-edge radius that is much smaller than the nose, wing, or vehicle length scale, while "blunt" implies the converse.

Sharp leading edges help reduce the vehicle's drag, enhance maneuverability and performance, and also improve safety due to an increased cross-range capability.[17] The WLE of the Space Shuttle orbiter has a radius of approximately 10 cm at the tip, while design concepts for some hypersonic maneuvering vehicles, such as the one under development in Defense Advanced Research Projects Agency (DARPA)'s Falcon program, have leading-edge radii on the order of millimeters. The challenge with sharp WLE designs is that the convective heating to the surface, and hence the surface temperature, increases as the WLE radius decreases. The surface temperature on the stagnation region of such sharp leading edges can potentially exceed 2000 °C (3632 °F). Few materials can survive extended periods at these temperatures and retain their dimensional and structural integrity in an aggressive oxidizing flow environment.

The performance advantage of diboride-based UHTC materials comes not only from their high-temperature capability, but also from their high thermal conductivity. Convective energy

* Corresponding author. Tel.: +1 650 859 2667; fax: +1 650 859 6196.
E-mail address: jochen.marschall@sri.com (J. Marschall).

0955-2219/$ – see front matter © 2010 Elsevier Ltd. All rights reserved.
doi:10.1016/j.jeurceramsoc.2010.01.026

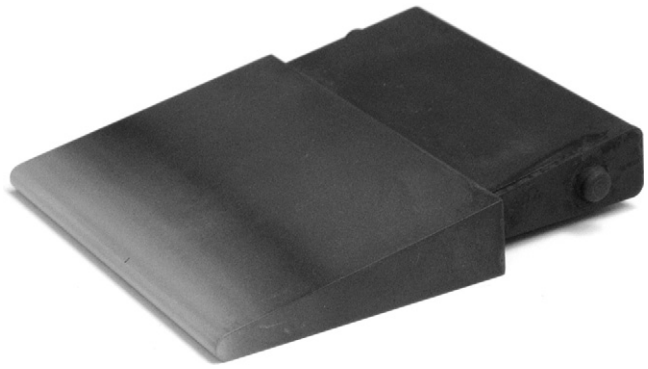

Fig. 1. UHTC wing leading-edge arcjet model.

that enters the surface near the stagnation region is conducted away to cooler regions of the leading edge, where it can be radiated back to the environment (Fig. 2). The higher the thermal conductivity of the leading-edge material, the more efficient this process becomes.[18] The UHTC leading edge then behaves much like a passive heat pipe, to move energy through, and eventually out of, the system.

The hypersonic applications of UHTC materials involve complex interactions between the material and the aerothermodynamic environment. Although most designers would choose to build concept vehicles and conduct flight tests in relevant environments, such testing opportunities are rare, often impractical, and always very expensive. Consequently, the design process for UHTC components for hypersonic vehicles is heavily dependent on computational methods and ground-based testing. Analytical performance predictions and the interpretation of ground-based testing require a self-consistent set of accurate material properties with well-defined uncertainties. Because UHTC components have to operate in environments from room temperature to nearly 2000 °C (3630 °F), it is important that most UHTC properties be measured over this entire temperature range.

The purpose of this paper is to describe the material properties that are most important for UHTC component design and the reasons why. Section 2 provides a brief introduction to hypersonic aerothermodynamics; to understand why a UHTC material might be used in a hypersonic application, materials developers must have at least a basic understanding of the hypersonic flight environment. Section 3 provides an overview of the design process and how it is influenced by material property uncertainties. Section 4 describes general materials information useful for designers and analysts. Section 5 discusses specific material properties and how they influence the design and analysis of the UHTC components. Section 6 provides a simple numerical example of how property uncertainties can impact the design space. Finally, Section 7 summarizes the conclusions and provides recommendations to UHTC material developers.

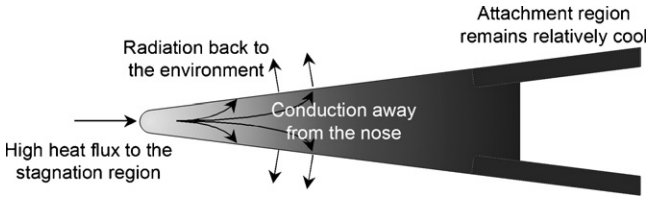

Fig. 2. UHTC leading-edge thermal management concept.

2. Summary of hypersonic aerothermodynamics

The analysis, design, and testing of UHTC components is driven by the hypersonic aerothermodynamic environment in which they are to be used. Generally, the term "hypersonic" refers to speeds in excess of Mach 5, or more than five times the speed of sound in the gas medium. Vehicles transiting an atmosphere at hypersonic speeds are exposed to extreme convective heating from high-enthalpy gas flowing past the vehicle. In some flight regimes, radiative heating for hot gases can also be important. This section serves as a brief introduction to the fundamental aspects of hypersonic flow.

2.1. Shock and boundary layers

At hypersonic speeds, a bow shock forms in front of the nose tip or WLE (Fig. 3). The stagnation point is the location on the leading edge, facing directly into the flow. The shock standoff length defines the distance between the bow shock and the stagnation point. Gases passing through the bow shock are compressed and increase in density, pressure, static enthalpy, and temperature. At sufficiently high enthalpies, the gas may become dissociated and ionized. In air, dissociation means that the N_2 and O_2 molecules break apart to become highly reactive N and O atoms. Because of their lower bond energy (5.1 eV vs. 9.8 eV), O_2 molecules dissociate at lower enthalpy levels than N_2 molecules. The exothermic recombination of these atoms at the surface can contribute significantly to the total aerothermal heating experienced by a component, depending on the particular flight or test environment.

When the high-enthalpy gas formed in the bow shock impinges on the leading edge, a boundary layer forms along the surface of the component (Fig. 3). The boundary layer region is characterized by large temperature, momentum, and chemical composition gradients normal to the surface. The gas flow is decelerated at the stagnation point, forming a thin boundary layer and a local subsonic region. The boundary layer thickens as the flow is redirected and accelerates around the WLE or nose

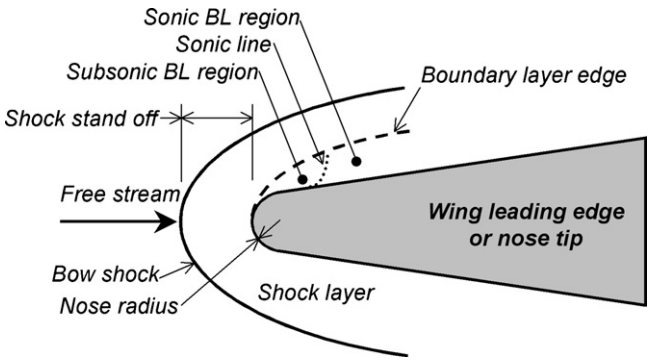

Fig. 3. Hypersonic flow features.

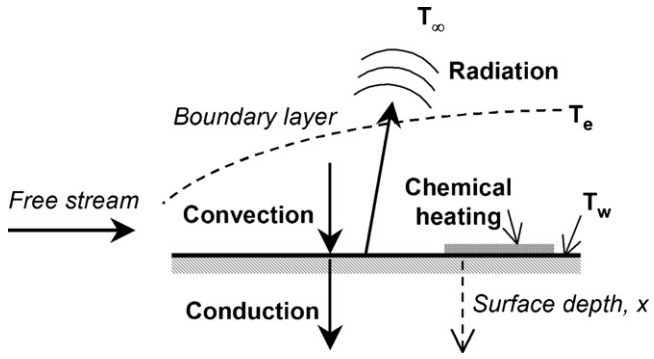

Fig. 4. Surface energy balance.

tip, regaining supersonic velocities. Boundary layer conditions determine local convective heating to the surface. Convective heating is typically highest in the stagnation point region and decreases, often significantly, away from the stagnation point.

2.2. Surface energy balance

The wall temperature on a hypersonic vehicle is determined by an energy balance that accounts for all of the heat transfer processes transporting energy into and out of the surface. Fig. 4 is a schematic of a steady-state energy balance at the surface, considering convective heating from the boundary layer, chemical heating from surface recombination reactions, re-radiation into the ambient environment, and conduction into the interior of the material.

The sensible convective heat flux to the surface, $\dot{q}_{\text{conv}}$, can be defined as a function of the gas enthalpy at the edge of the boundary layer, h_e, the enthalpy of the gas at the wall, h_w, and a transfer coefficient, C_H. The expression for convective heat flux can be written as:

$$\dot{q}_{\text{conv}} = C_H[h_e(T_e) - h_w(T_w)], \tag{1}$$

where T_e is the boundary layer edge gas temperature and T_w is the temperature of the wall (surface).

The transfer coefficient is a function of the boundary layer conditions, which are dependent on the free-stream conditions (speed, temperature, and pressure), the gas composition, and the geometry of the leading edge. The transfer coefficient is also a function of whether the boundary layer flow is laminar or turbulent. Turbulence can significantly increase the convective heating to the surface. Hypersonic aircraft are usually meticulously designed to avoid turbulent flow and prevent laminar boundary layers from becoming turbulent. The roughness of the surface material can be a critical aspect of transition to turbulence; this will be addressed in Section 5.

High levels of dissociated gases can be present in flight and also in the free streams of high-enthalpy test facilities, including arcjets and inductively coupled plasma wind tunnels, such as the Plasmatron at the von Karman Institute for Fluid Dynamics in Belgium. The diffusion of these species to the surface, and their exothermic heterogeneous reaction on or with the surface material, can transfer additional energy to the surface. Gas–surface chemical interactions can be quite complex, and approximate computational models are almost always used. A simplified model of chemical heating that considers only independent oxygen and nitrogen surface recombination can be written as:

$$\dot{q}_{\text{chem}} = \gamma'_O(T_w)\frac{\Delta E_{\text{dis},O_2}}{2}\Gamma_O + \gamma'_N(T_w)\frac{\Delta E_{\text{dis},N_2}}{2}\Gamma_N, \tag{2}$$

where γ'_i is the total catalytic recombination efficiency, Γ_i is the surface impingement flux for reactant species i, and $\Delta E_{\text{dis},j}$ is the dissociation energy of product j. The total catalytic recombination efficiency (γ'_i) is the product of the species recombination efficiency, γ, and the energy accommodation efficiency, β. The species recombination efficiency (γ) is the fraction of collisions with the surface that result in loss of the reactant from the gas phase, and the energy accommodation efficiency (β) is the fraction of exothermic reaction energy that is transferred to the surface. For independent reactions γ', γ and β may all vary from a minimum of 0 to a maximum of 1. The surface impingement flux, Γ_i, is typically taken as the gas kinetic expression $n_i\sqrt{RT_w/2\pi M_i}$, where R is the universal gas constant, and n_i and M_i are the number density and molar mass of the reactant, respectively.

The re-radiation away from the surface is a function of the wall temperature, the environment temperature, T_∞, the Stefan–Boltzmann constant, σ, and the emissivity, ε, and can be expressed by the Stefan–Boltzmann relationship:

$$\dot{q}_{\text{rad}} = \varepsilon(T_w)\sigma[T_w^4 - T_\infty^4]. \tag{3}$$

The emissivity may vary from 0 to 1; $\varepsilon = 1$ for a perfect blackbody radiator.

Energy conduction into the interior is a function of the local temperature gradient into the surface and the thermal conductivity, k, of the material through Fourier's law:

$$\dot{q}_{\text{cond}} = -k(T_w)\left.\frac{dT}{dx}\right|_w. \tag{4}$$

The steady-state surface energy balance equates the total aerothermal heating of the surface ($\dot{q}_{\text{conv}} + \dot{q}_{\text{chem}}$) to the energy transferred away from the surface ($\dot{q}_{\text{rad}} + \dot{q}_{\text{cond}}$):

$$C_H[h_e(T_e) - h_w(T_w)] + \gamma'_O(T_w)\frac{\Delta E_{\text{dis},O_2}}{2}\Gamma_O + \gamma'_N(T_w)\frac{\Delta E_{\text{dis},N_2}}{2}\Gamma_N = \varepsilon(T_w)\sigma[T_w^4 - T_\infty^4] - k(T_w)\left.\frac{dT}{dx}\right|_w \tag{5}$$

The surface energy balance can be used to compute the surface temperature, given the conditions of the flow, environment, and material properties. The actual solution of the expression is complicated by the fact that the properties of real materials, such as UHTCs, are functions of temperature. Moreover, Eq. (5) is a simplification of the more general case, which might also include radiation transfer to the surface from hot gases in the shock layer, more complicated surface reactions, as well as energy storage effects associated with transient heating conditions. Generally, the solution is part of a large numerical thermal analysis using computational fluid dynamics (CFD) programs

and involving multi-dimensional geometry and time-dependent boundary conditions that are usually provided by an independent solution of the flow field and boundary layer.

The significance of Eq. (5) for material scientists is that the surface temperature experienced by a UHTC component during hypersonic flight or high-enthalpy flow testing is determined not only by the environment and vehicle or component shape, but also by temperature-dependent material properties, such as emissivity, thermal conductivity, and catalytic efficiency (as well as absorbance and heat capacity in the more general case).

2.3. Approximate analyses and estimates

Because of the coupled nature of the surface energy balance, complicated numerical analyses are typically required for accurate solutions. However, two approximate analyses are in common use, particularly in the early stages of vehicle or mission design.

Hypersonic aerothermal environments are often quantified in terms of a heat flux to the vehicle surface. For example, vehicle designers may specify that a candidate leading-edge material must sustain a particular peak stagnation point heating rate. The transfer coefficient and boundary layer edge temperature are relatively insensitive to the thermal conditions at the wall and are often predicted independent of the wall conditions, using CFD codes or engineering correlations, together with information about the free-stream conditions and the nose tip or WLE geometry. One common approximation for the aerothermal heat flux is to ignore the surface energy balance and calculate heating directly from the left hand side of Eq. (5), assuming a fixed, low-wall temperature, typically 300 K, and fully catalytic behavior ($\gamma' = 1$).

The heat flux defined in this way is referred to as $\dot{q}_{\mathrm{fc,cw}}$, a "fully catalytic cold-wall" heat flux. The advantage of this definition is that $\dot{q}_{\mathrm{fc,cw}}$ is only a function of the flow conditions (free stream and geometry) and is completely independent of the surface thermal conditions. It provides a common reference point for the comparison of different flow environments. In a sense, the fully catalytic cold-wall heat flux represents the energy in the environment that is potentially available to heat the surface. Usually, when aerospace engineers or aerothermodynamicists refer to the "peak heat flux" in a hypersonic flight regime, they are referencing to a fully catalytic, cold-wall value. The fully catalytic, cold-wall heat flux is always higher than the corresponding hot-wall flux in flight, as surface temperatures in flight will typically be much hotter than 300 K, and real materials are not fully catalytic.

The distinction between cold-wall and hot-wall heat flux is also important when evaluating material performance in ground-test environments. For example, test conditions in arc-jet or Plasmatron wind tunnels are routinely characterized using water-cooled copper calorimeters, whose surface temperatures remain near room temperature during the measurement.[19,20] Such a measurement is essentially a cold-wall heat flux measurement on a highly catalytic surface. The heat flux experienced by the test specimen under the identical flow conditions will be a hot-wall heat flux, on a surface that is probably much less catalytic than copper.

A second common approximation, useful for quickly estimating thermal response to a prescribed heat flux, is the "radiation equilibrium temperature." This approximation simplifies the surface energy balance by assuming negligible heat conduction into the material ($\dot{q}_{\mathrm{cond}} = 0$) and a constant value for aerothermal heat flux, often a fully catalytic, cold-wall heat flux value obtained as described above. With these assumptions, the energy balance can be rearranged as an algebraic equation for T_{w}:

$$T_{\mathrm{w}} = \sqrt[4]{\frac{\dot{q}_{\mathrm{fc,cw}}}{\varepsilon\sigma} + T_{\infty}^{4}}. \tag{6}$$

Since Eq. (6) ignores the effect of heat conduction into the interior, the radiation equilibrium temperature generally represents the maximum potential surface temperature for a given heat flux condition, assuming a conservative (low) value of surface emissivity is used. The radiation equilibrium temperature can be a valuable engineering level tool for quickly estimating thermal response and as a sanity check for validating computational analyses. However, the approximation of zero heat conduction is generally not valid for materials with relatively high thermal conductivities, such as metals or UHTCs. As discussed previously, high thermal conductivity is one of the enabling properties of diboride-based UHTC materials, because it allows heat to be drawn out of the stagnation region and re-radiated from a larger surface area. Thus, a radiative equilibrium temperature may significantly overestimate the steady-state surface temperature in the stagnation point region of a sharp UHTC nose tip or WLE.

2.4. Computational methods

Predicting the aerothermal conditions and material thermal response of a UHTC component in a hypersonic vehicle design usually requires the application of numerical computations. Even for simple sphere–cone geometries, the flow conditions and thermal response are too complex to evaluate with direct analytical methods. In a real aerothermal flight environment, the thermal conditions at the material surface and the boundary layer conditions are interdependent. However, for dimensionally stable (non-ablating, non-pyrolyzing) thermal protection systems, this interaction is often weak, when compared to the effect that the free-stream flow conditions and vehicle shape have on the boundary layer. Under these conditions, it is preferable to perform design computations in which the numerical analyses of the flow conditions and the material thermal response are performed independently—and in which the interface between the fluid and solid regions is treated as a boundary condition in each of the independent analyses.

NASA uses computational fluid dynamics programs, such as the Data Parallel Line Relaxation (DPLR) program[21] or the Langley Aerothermodynamic Upwind Relaxation Algorithm (LAURA),[22] to predict the flow conditions around a vehicle traveling a particular flight trajectory through the atmosphere. These programs solve the Navier–Stokes equations and can predict the dynamic, thermodynamic, and chemical conditions in the shock

layer and boundary layer, as well as provide the surface heat flux as a boundary condition to the materials response model. Material response analyses employ finite-difference, finite-volume, or finite-element methods to perform computations as a function of transient heating. NASA Ames Research Center uses the commercial finite-element MSC.Marc package[23,24] to predict the transient surface and in-depth thermal response of UHTC nose tip and WLE components. Other researchers have used the commercial codes ABAQUS,[25] COMOS/M, COSTAR,[26] and ANSYS[27,28] to model UHTC thermal and mechanical response.

The complexity associated with the prediction of material response along a flight trajectory is highly dependent on the level of coupling between the flow field and material analyses. Decoupled solutions are obtained by setting surface temperatures to either cold-wall or radiative equilibrium values in the CFD analyses and then using the computed transient convective heating profile as a boundary condition to a material response model. In this approach, no material properties are required for the flow field analysis, if the surface temperature is set to an arbitrary cold-wall value, and only the surface emissivity is required if the radiative equilibrium temperature assumption is used. Although the radiation equilibrium temperature generally over predicts the actual surface temperature, the estimate is usually much closer than assuming a cold-wall.

However, for sharp UHTC components, the combination of high thermal conductivity, multi-dimensional heat conduction, and significant volumetric heat capacity, often necessitates some level of coupling between the flow field and material response computations, in order to achieve time-accurate predictions for temperature and stress in a transient aerothermal heating environment. Loose coupling is achieved by incrementing flow field and material response computations sequentially during each time step, while full coupling requires the iterative solution of the flow field and material responses to satisfy the full surface energy balance during every time step. For trajectory-based design space studies, solution of the full Navier–Stokes equations is sometimes replaced by more approximate analytic-flow correlations and boundary layer solutions to make the computations more tractable.[24] Requirements for the level of coupling to achieve time-accurate solutions for UHTC components are discussed in the literature.[24,29,30]

3. The design process and property uncertainty

Hypersonic vehicle designs are driven by mission objectives that demand certain performance criteria. Designers attempt to fulfill these criteria in a constrained optimization process, adjusting the shape and mass of a vehicle to achieve the desired flight characteristics, while simultaneously remaining within bounds imposed by the properties of available aerospace materials. Material property uncertainties, along with the variations or dispersions in the other parameters, such as aerothermal heating or aerodynamic loads, are used to define the design space, assess the design against system requirements, and determine margins or factors of safety. Components and systems must "buy" their way onto a vehicle design by proving that they are lower risks than competing systems. Reducing uncertainties in material properties reduces the risks in the design—risks associated with component failure, mission failure, or loss of the vehicle. The aerospace industry maintains standards that define the design process and the role that material properties play in that process. NASA has developed its own standards for the design and assessment of spaceflight hardware and thermal protection system design.[31–34]

An important early step in the design process is defining and selecting the specific set of material property values that will be used in analyses. The design team must evaluate different data sources and select the data sets deemed most directly applicable and reliable for the given application. Often this step includes down selection from a large property database, like NASA's TPS*X* Material Properties Database.[35] The availability and quality of property uncertainties associated with different data sets is always a key criterion for this down-selection process. At this stage, the lack of quality uncertainty information or specific experimental data often dictates that new property measurements be made.

Material property data are usually provided as either compiled statistical values, such as a mean and standard deviation on a particular property, or as a set of data points from which the statistical values can be derived. It is typical for designers to use bounding values of ± 3 standard deviations (3σ) to define the dispersions in the design. A large variation in a measured property may mean that the 3σ values push some design parameters beyond acceptable limits. Some specific approaches for the use of property uncertainty data include performing sensitivity studies, in which material properties are parameters that are varied in a regular pattern to ascertain their effect on the thermal and mechanical response of the system. A common application of this approach is to assess the system with a "worst-on-worst" combination of material properties and flight loads. Another approach uses a Monte Carlo simulation to run a large number of analyses, randomly varying material properties and other design parameters based on their nominal values and standard deviations.[36] These analyses are very effective for identifying the parameters that have the largest influence on the system performance.

4. General material information

Before proceeding to a discussion of specific material properties used in design computations, it is helpful to outline the general material information that designers and analysts need when developing hypersonic vehicles. This information is useful in assessing the results of analyses or in determining the potential applicability of a material.

4.1. Sources of uncertainty

Multiple tests for the same material property usually yield a distribution of values, even for relatively easy-to-measure properties such as density. Designers need to know these distributions, in order to define bounding cases and dispersions in the design space. Distributions in material properties arise from a variety of sources, including manufacturing variability, the use

of different techniques to derive the same material property, and inherent uncertainties in different measurements techniques.

No material manufacturing process is perfectly reproducible. Lot-to-lot variations are expected and tolerated (within certain limits). UHTC materials are certainly no exception to this rule. Manufacturing processes, such as hot pressing of ceramic powders, are defined by a large number of variables that can only be controlled within certain tolerances. Even under nominal processing conditions, acceptable material lots will have properties that vary about some average value. It is also common for materials manufactured in a pressing, molding, or casting process to exhibit non-uniform material properties within a single billet. Such non-uniformities can occur, for example, near surfaces, due to interactions with die or mold surfaces, or along directions aligned with the application of stresses or gravity that cause segregation of constituents.[12] It is important for materials researchers to quantify both inter-billet and intra-billet property distributions.

Whenever possible, multiple material property measurements should be made on specimens from the same billet or manufactured from the same lot of starting material. Such data are more valuable than properties measured on specimens from different starting billets or material lots, because they allow material developers and vehicle designers to determine correlations among material properties and to estimate trends in manufacturing.

Consistency in test specimens is also important for any material property derived from combinations of separate test data. For example, the thermal conductivity is related to the density, ρ, specific heat, c_p, and thermal diffusivity, α, by the relationship:

$$k = \alpha \rho c_p. \tag{7}$$

Thermal diffusivity is often measured directly at high temperature using laser-flash techniques,[37] but it is usually thermal conductivity that is required as an input to thermal analysis programs. The thermal conductivity must then be derived from the measurements of density, specific heat, and diffusivity, and if these properties are measured on unrelated samples, the calculation of thermal conductivity may result in inconsistent values at best, or, even worse, significantly inaccurate values.

Many material properties can be measured with a variety of experimental techniques. Often these techniques and their associated data reduction procedures are quite different. For example, tensile modulus can be measured by acoustic techniques or mechanical tests; fracture strength can be measured in tension, compression, or bending geometries; thermal conductivity can be obtained directly using steady-state methods like guarded hot-plate testing, or indirectly, by transient methods like laser-flash or photothermal radiometry, which measure thermal diffusivity.

It is important to describe or reference measurement methods well, so that informed judgments can be made and discrepancies among different property values resolved. In this regard, standard measurement techniques, such as those defined by the American Society for Testing and Materials (ASTM), are desirable, because both the measurement procedure and uncertainty are defined in the standard. The use of nonstandard techniques should be avoided, whenever possible, because uncertainty is more difficult to assess.

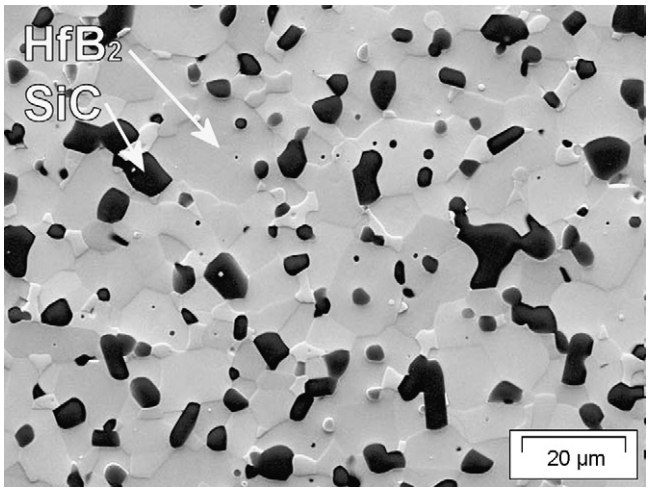

Fig. 5. Scanning electron micrograph of a HfB_2 UHTC composite containing 20 vol.% SiC; the light grains are HfB_2 and the dark grains are SiC.

In summary, the more information supplied to the designer about how a property was measured and what sources of uncertainty are incorporated into quoted errors, the tighter the resulting design space. Missing information inevitably forces analysts to assume conservative uncertainties that may vastly exceed those that actually exist.

4.2. Material morphology

UHTC materials are often referred to as monolithic and are treated as having homogeneous properties. But a micrograph of an HfB_2-SiC UHTC sample (Fig. 5) clearly shows the composite nature of the material. Microstructure significantly influences the properties of a material through the distribution of different material phases and the location and size of defects and voids. Information about material microstructure can help analysts interpret the macroscopic performance of the material and is particularly useful in understanding and predicting failure modes.

An important aspect of material morphology is the introduction of anisotropic material properties. Many aerospace materials, such as carbon fiber composites or rigid ceramic tile insulations, exhibit direction-dependent thermal and mechanical properties. Generally, these materials fall into two categories: orthotropic materials with properties oriented in three mutually orthogonal directions, and transverse isotropic materials, with properties oriented in two orthogonal directions, though-the-thickness and in-plane. Most hot-pressed UHTCs are treated as isotropic in analysis and design, but it is important for material developers to investigate the directional dependence and verify that the isotropic assumption is valid. Failure to incorporate significant orthotropic or transverse isotropic properties in analyses can lead to erroneous predictions of thermal and mechanical performance and, ultimately, poor component design.

4.3. Material use limits

Some material parameters are not measured directly, but are determined by material performance. Maximum temperature limits and maximum stress limits are examples of such parameters. Designers need to establish these limits based on an analysis of a collection of material properties and behaviors.

Obviously, the extreme upper temperature limit is set by a material's melting point or eutectic temperature. However, a hypersonic vehicle designer will never expect to use a material up to that temperature. Instead, the designer needs to define a practical temperature limit beyond which the thermal, mechanical, and other properties are potentially degraded to such a point that the material can no longer perform its required function. The material composition, although not used directly in design computations, can be useful information in defining capabilities and material limits. For example, if any of the material components are susceptible to oxidation, it is important to know the temperature at which oxidation rates become significant. Such information would not be used directly in a computational analysis, but may affect the operational limits of the vehicle or may demand that components be coated with an oxidation barrier.

The mechanical performance constraints may be associated with more than one type of stress limit, depending on the mode of loading: tensile, compressive, or shear. Maximum stress limits are usually obtained from mechanical failure data. While the thermal and electrical properties of UHTC materials are somewhat "metallic" in nature, the failure characteristics are more typical of the brittle fracture of a ceramic. Most fracture strength data on UHTC materials are obtained in flexure testing.[10,12,38–42] UHTC fracture strengths tend to decrease with increasing temperature.

Because it is difficult to perform failure-prediction analyses of brittle materials, analysts generally perform standard mechanical or thermal/mechanical analyses and then compare the predicted stress results with experimentally measured mechanical strength values. For brittle materials, this may be in the form of statistical data, such as the Weibull modulus.[12,43] Designers will usually apply some factor of safety to the strength values and use those margined values for comparison with mechanical analyses. If mechanical strength data are not accurate or extensive enough to generate robust statistics, the designers may be required to apply a higher factor of safety to cover the uncertainty, which can lead to overly conservative designs.

In general, material developers need to provide enough accurate material property data under sufficiently stressful testing conditions so that proper use limits can be established to within an acceptable uncertainty. Testing UHTC materials and components at very high temperatures and past the point of failure are import aspects of material characterization.

4.4. Properties not used in component analyses

There are many properties commonly reported for UHTC materials that are not directly useful for thermal or mechanical analyses. Some examples are hardness or microhardness[5,12,44,45] fracture toughness,[10,39,41,46–49] and thermal shock parameters.[5,11,50] These properties can be valuable indicators for tracking processing-related changes and for optimizing desired properties or capabilities in UHTC materials. They can also be helpful when screening candidate materials for particular applications and for assessing performance issues, such as damage resistance during handling or shipping. However, properties like hardness, fracture toughness, and thermal shock resistance, are of marginal importance in design computations, as their numerical values are never input directly into any analyses.

5. Specific material properties

The design and analysis of UHTC components for hypersonic applications ultimately require numerical values of specific physical, thermal, mechanical, and surface properties. The important material properties discussed below appear directly in either boundary conditions like Eq. (5) or in governing equations for heat transfer and mechanical equilibrium. Some examples of governing equations for an isotropic material are the energy conservation equation:

$$\rho c_{\mathrm{p}} \frac{\partial T}{\partial t} = \frac{\partial}{\partial x}\left(k\frac{\partial T}{\partial x}\right) + \frac{\partial}{\partial y}\left(k\frac{\partial T}{\partial y}\right) + \frac{\partial}{\partial z}\left(k\frac{\partial T}{\partial z}\right), \tag{8}$$

which relates the energy storage rate to heat flux gradients within a material, and Hooke's law:

$$\begin{bmatrix} \varepsilon_{xx} \\ \varepsilon_{yy} \\ \varepsilon_{zz} \\ \varepsilon_{yz} \\ \varepsilon_{zx} \\ \varepsilon_{xy} \end{bmatrix} = \frac{1}{E} \begin{bmatrix} 1 & -\nu & -\nu & 0 & 0 & 0 \\ -\nu & 1 & -\nu & 0 & 0 & 0 \\ -\nu & -\nu & 1 & 0 & 0 & 0 \\ 0 & 0 & 0 & 1+\nu & 0 & 0 \\ 0 & 0 & 0 & 0 & 1+\nu & 0 \\ 0 & 0 & 0 & 0 & 0 & 1+\nu \end{bmatrix} \begin{bmatrix} \sigma_{xx} \\ \sigma_{yy} \\ \sigma_{zz} \\ \sigma_{yz} \\ \sigma_{zx} \\ \sigma_{xy} \end{bmatrix}, \tag{9}$$

which relates the elastic strains, ε_{ij}, and stresses, σ_{ij}, within a material through the tensile modulus, E, and the Poisson's ratio, ν.

Because UHTC materials in hypersonic vehicle applications are required to operate at very high temperatures, designers and analysts will require that most of the properties discussed below be provided as a function of temperature over the entire temperature range of interest. Measuring material properties at high temperatures is always difficult and sometimes impossible. In such cases, material developers should provide estimates of high-temperature properties based on engineering judgment, similarity with other materials, or extrapolation of existing data. Whatever approach is used, an estimate of the uncertainty or error in the high-temperature properties should also be provided.

5.1. Physical properties

The most important physical properties for UHTC materials are the density and the coefficient of thermal expansion (CTE).

Density appears as a first-order term in the governing equations for thermal and dynamic mechanical response (for example, vibration). Because variations in density have a large

effect on the thermal and dynamic mechanical performance of components, material developers should provide as accurate a value as possible with as tight a tolerance as possible. It should be possible to make individual density measurements with measurement errors less than 1%. Density also determines the mass (weight) of a component, which is always a critical aspect of the design. UHTC materials are much denser than typical aerospace materials, such as carbon composites or aluminum alloys, and managing the total and distributed mass of a vehicle is one of the most important functions of the designer. Typical designs for UHTC wing leading edges and nose tips require very little material, due to the high temperature capability and high thermal conductivity. Additionally, the location of the high density UHTCs at the forward end of the vehicle can have the beneficial effect of moving the center of gravity further forward, which often results in better aerodynamic stability.

Most materials exhibit changes in density as a function of temperature associated with thermal expansion. The effects of density changes on heat transfer performance are usually negligible. In the analysis of thermo-mechanical responses, the thermal expansion behavior of a material is typically incorporated in the linear coefficient of thermal expansion (CTE). The CTE is a critical material property. Local thermal expansion within a UHTC component can produce large internal strains and stresses, particularly under conditions that cause rapid temperature changes. Differential thermal expansion between a UHTC component and a neighboring material can cause undesirable contact stresses. Thermally induced stresses often limit the size and shape of a UHTC component. When predicted thermal stresses approach maximum allowable stress limits, conditions for thermal shock failure exist and components may have to be redesigned to dissipate heat more effectively. This generally means making smaller UHTC components with lower aspect ratios. For non-isotropic materials, the CTE must be provided in each of the primary material directions.

The CTE is usually derived from measurements of the elongation of a material at elevated temperatures. Because the CTE is the first derivative, or slope, of the curve of elongation versus temperature, measurements must be performed with sufficient resolution to extract this derivative, without introducing undesirable artifacts into the CTE values. The CTE can also be obtained for pure crystalline materials using X-ray diffraction techniques to measure changes in lattice constants with temperature. Often the thermal expansion behavior over a large temperature range is non-linear and must be defined by several average CTE values over sequential temperature intervals. Typical CTE values for ZrB_2 and HfB_2 composites lie in the $5–8 \times 10^{-6}\,K^{-1}$ range, with the higher values found at higher temperatures.[11,12,48,49,51]

5.2. Thermal properties

The most important thermal properties for UHTC materials are the specific heat and the thermal conductivity. Both properties appear as first-order terms in the governing conservation-of-energy equation.

The specific heat can have a large effect on the transient thermal response of a UHTC component during heating or cooling. Specific heat is generally a strong function of temperature for UHTC materials, particularly from room temperature up to $\sim$1000 °C. For example, the specific heat of HfB_2 increases by about a factor of two over this temperature range.[52] While specific heat values for composite materials can be estimated from measurements performed on isolated constituents, values measured directly on the actual material are much preferred. Sample volumes used in calorimetry are often small. For UHTC composites, it is important to ensure that the samples used for specific heat measurements accurately reflect the composition of the bulk material. During high-temperature calorimetry, the absence of chemical reactions between UHTC constituents and sample containers must be verified.

Thermal conductivity exerts a dominant effect on heat transfer and coupled thermo-mechanical responses and is a particularly important property for sharp UHTC leading-edge components, as the ability to conduct heat away from sharp edges is an enabling characteristic. In general, thermal conductivity can be directionally dependent. If a material exhibits anisotropic behavior, analysts will require thermal conductivity values for all of the primary material orientations.

UHTC materials exhibit thermal conductivities with a wide range of magnitudes and a variety of temperature dependencies.[3,52] Because the thermal conductivity of UHTC composites depends on many different factors, including microstructure, composition, defect and impurity levels, contact resistance between grains, and porosity, values cannot be estimated with any confidence from published data or measurements performed on individual constituents. Even nominally similar UHTC composites may not have the same heat transport characteristics, because the factors that affect thermal conductivity are largely determined by manufacturing details, for example, the raw ceramic powders sources, powder processing procedures, and hot-pressing schedules.[12,52] Thus thermal conductivities over the entire temperature range of interest must be measured for the exact UHTC material to be used in a particular component application.

Since most high-temperature thermal conductivity values are actually derived from thermal diffusivity measurements (as previously described), it is important that the specific heat and density values required to extract thermal conductivity from thermal diffusivity be measured on the same lot of UHTC material, preferably the same test specimen, if possible. Typical uncertainties reported for direct UHTC thermal property measurements are ±3% for specific heat,[13,53,54] ±5% for thermal diffusivity,[13,53] and ±5% for thermal conductivity.[55] These uncertainties are associated with measurement technique and the consistency of repeated measurements on the same sample and do not include multiple sample statistics. Note also that if thermal conductivity is calculated from $k = \alpha \rho c_p$, uncertainties in the contributing properties combine and propagate.

5.3. Mechanical properties

The primary mechanical properties required for analyses of isotropic UHTC components are the tensile modulus and the Poisson's ratio. Both appear as first-order terms in the governing

static equations. For isotropic materials, the shear modulus, G, can be calculated from the tensile modulus and Poisson's ratio as $G = E/[2(1+\nu)$ and does not have to be independently specified.

The tensile modulus (also called the Young's modulus or elastic modulus) has a large effect on the mechanical response of the component. Ideally, tensile modulus values are derived from the slope (or first derivative) of a material's stress–strain curve under uniaxial tension in the elastic loading regime. However UHTC materials have very limited ductility, and their tensile moduli are almost always either measured by acoustic methods or derived from experimental stress–strain curves obtained during flexure testing. The flexure method was found to produce somewhat lower (by ~15%) values for some UHTC materials than the tensile and acoustic methods.[3,56]

Tensile modulus values can be used directly in mechanical analyses, but it is often more accurate to incorporate the actual stress–strain relationship. Most analytical software packages can handle inputs of either type. Incorporating the experimental stress–strain curve is particularly advantageous for materials that exhibit non-linear elastic response or for when the experimental stress–strain curve contains plastic strain contributions deemed important for a particular application. Non-linear, elastic deformation behaviors are observed for some UHTC materials at elevated temperatures.[3,40–42,57] The tensile modulus magnitude tends to decrease with increasing temperature. Accurate temperature-dependent modulus data are desirable, but difficult to measure. In practice, if the expected thermal and load environments combine to push a UHTC component into a highly non-linear or highly temperature-dependent mechanical property regime, a redesign of the component or system is likely.

The Poisson's ratio is defined as the ratio of lateral contraction to axial extension under uniaxial loading. It can be measured during a uniaxial tensile test or by acoustic methods. Although the Poisson's ratio does not often have a large influence on the magnitude of predicted stresses and strains in a component, it can significantly affect the distribution and orientation of those stresses and strains. This is particularly important when modeling three-dimensional sharp components subjected to large temperature gradients. Typical values for metals are around 0.3; UHTC materials generally have lower Poisson's ratios, in the 0.1–0.2 range at room temperature.[10,11,39] The Poisson's ratio does not tend to be highly temperature dependent for real materials, so analysts do not usually require temperature-dependent values.

The number of mechanical properties that must be measured increases rapidly with anisotropy. For transverse isotropic materials, two tensile moduli, two Poisson's ratios, and one shear modulus are required, and for orthotropic materials, three tensile moduli, three Poisson's ratios, and three shear moduli are required. As with the tensile modulus, it is desirable to define the temperature-dependent behavior of the shear modulus, but estimates of that behavior are often good enough.

5.4. Surface properties

The three most important surface properties for UHTC materials are the emissivity (or emittance), the catalytic efficiency, and the surface roughness. The first two properties enter into the surface energy balance, while the third influences laminar-to-turbulent transitions in the boundary layer flow.

In the general case, emissivity is a function of wavelength, emission direction, and temperature. The total hemispherical emissivity – a value averaged over all wavelengths and emission directions – is required in the surface energy balance. Because emissivity acts as a multiplicative coefficient to the Stephan–Boltzmann radiation function, it has a large effect on the ability of the surface to reject heat, and thus, on the steady-state surface temperature reached by a component. The total hemispherical emissivity can be a strong function of temperature; so temperature-dependent emissivity values are usually required. Direct measurements of hemispherical emissivity at elevated temperatures are difficult, and few such data are available in the literature for UHTC materials. The measurements of Scatteia et al.[58,59] for ZrB_2–15SiC–2$MoSi_2$, ZrB_2–15SiC, and ZrB_2–15SiC–10HfB_2 composites are a notable exception. Emissivity values ranged from 0.49 to 0.81, depending on material composition, temperature, machining method, and ambient oxygen environment. Scatteia et al.[58,59] assign errors of ±5% to their measurements.

Often temperature-dependent emissivity values are estimated from room-temperature hemispherical spectral reflectance measurements.[60] We use optical relations for an opaque solid and Kirchhoff's law to obtain spectral emissivity from the measured spectral reflectance and then average the spectral emissivity over the Planck function at different temperatures to compute temperature-dependent total emissivity values. It is difficult to assign rigorous uncertainties to this process.

An *in situ* emissivity measurement can be made during testing in high-enthalpy facilities by simultaneous one-color and two-color radiometry, wherein the surface temperature is determined by the two-color measurement, and the emissivity is derived from the one-color measurement, using the known surface temperature. A value of 0.9 was reported by Monteverde and Savino[61] for ZrB_2–15SiC samples, using this technique. However, this emissivity is a directional value appropriate for the wavelength band of the one-color radiometer and cannot be used in the energy balance without introducing major uncertainty.

Design computations often assume that all atoms reaching the surface recombine (full catalytic recombination) and that all of the exothermic energy is released to the surface (full energy accommodation). These assumptions are extremely conservative for flight and can be very unrealistic when applied in analyses of ground tests. Temperature-dependent species recombination efficiencies for some UHTC materials have been measured in laboratory experiments.[58,59,62] Maximum values of $\gamma \cong 0.1$ were reported for oxygen atom recombination by Scatteia et al.[59] on ZrB_2–15SiC and ZrB_2–15SiC–10HfB_2 materials at 1800 K, indicating less than fully catalytic behavior. Scatteia et al.[58,59] assigned an uncertainty of ±30% to their species recombination coefficient measurements. The total catalytic efficiency γ' can be derived from heat flux and surface temperature measurements during arcjet or Plasmatron tests using CFD models.[60,63] At similar surface temperatures, Marschall et al.[60] found values of $\gamma' \cong 0.001$–0.002 for ZrB_2–30SiC surfaces during Plasmatron

exposure, which seems to indicate that energy accommodation is also not complete. Marschall et al. demonstrated that the uncertainty in deriving γ' by this approach can reach an order of magnitude and is greatly affected by the value of surface emissivity assumed in the analysis.

The surface roughness of the material can have profound effects on the boundary layer flow. Hypersonic vehicles with sharp nose tips and WLEs are designed to operate in laminar flow environments. If the laminar boundary layer should "trip" and become turbulent, the convective heating to the surface can increase dramatically. CFD tools employ analytical models and empirical correlation methods to predict roughness-induced transitions from laminar to turbulent flow and the induced turbulent surface heating. These correlations typically make use of "average" roughness heights,[64–66] derived from experimental distributions of roughness height and the peak-to-peak distance. Models that predict laminar-to-turbulent flow transitions only require the average distributed roughness height of the surface as an input. Once the flow has become turbulent, any large-scale surface roughness that rises above the laminar sublayer in the boundary layer can further augment the turbulent heating. Models to predict this augmented heating typically require the average peak-to-valley roughness height and the lateral spacing between the large roughness elements.

Note that surface properties can be strongly influenced by manufacturing techniques and tolerances, so that these properties should be measured on UHTC surfaces prepared in a similar manner as the prospective component. Additionally, exposure to a high-enthalpy flow can produce significant changes in the surface topology, microstructure, and chemical composition, as the result of oxidation reactions, volatilization processes, and phase changes. Therefore, emissivity, catalytic behavior, and surface roughness should be measured on both virgin materials and samples that have been exposed to surface heating conditions similar to those expected during flight. This is another reason why the use of arcjet and Plasmatron testing is critical to understanding the performance of UHTC components. To date, little research has been reported in the literature on the catalytic behavior, emissivity, and surface roughness of UHTC materials as a function of machining methods or environmental exposure.[58,59,62]

6. Computational example

To present a simple computational example illustrating the effects of property variations on the thermal and mechanical response of a UHTC component, we performed finite-element analyses on a representative WLE section exposed to a constant convective heat flux distribution. This distribution is based on a worst-case estimate of reentry conditions for a winged crew transfer vehicle.[67] The WLE cross-section is a cylinder-wedge configuration with a nose radius of 1 mm, a half angle of 5.6° and an overall length of the 76.2 mm (3 in.). Fig. 6 shows the WLE cross-section and the applied heat flux as a function of stream length coordinate (the distance along the surface starting at the stagnation point).

Transient solutions for the UHTC thermal and mechanical response to heating were obtained using MSC.Marc, a commercial fully non-linear finite-element analysis package. The finite-element grid was three-dimensional and used 28640 8-noded, bi-linear elements. The UHTC surface was allowed to re-radiate energy to an environment at 300 K. A node at the aft end of the WLE model was fixed to prevent rigid body movement; the rest of the model was then allowed to expand and contract without constraint. The mechanical analyses were quasi-static—at each time step the strain was predicted, based on the CTE and current temperature distribution. Table 1 shows the nominal physical, thermal, mechanical, and surface properties for a monolithic hot-pressed HfB_2/SiC composite used in the analyses.[12,43,52]

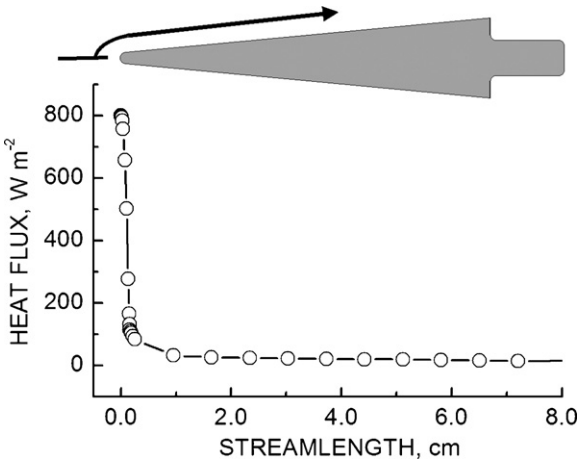

Fig. 6. Cross-section of model UHTC WLE and applied heat flux distribution.

Fig. 7a–d shows temperature, principal total strain maxima, principal tensile stress maxima, and shear stress maxima contours at the peak tensile stress time during heating (~7 s after application of the heat flux). While the strain contours follow the temperature contours closely, the coupled thermal/mechanical analysis reveals very different spatial distributions for temperature and stress in a complex three-dimensional part. The locations of the highest principal tensile stresses are not in the stagnation region of leading edge, which sees the highest heat flux and experiences the highest surface temperatures, but rather in the interior of the wedge away from the leading edge and the lateral wedge faces. The highest shear stresses occur at the sides of WLE towards the leading edge and do not coincide with the locations of the highest tensile stresses.

Fig. 8 shows how the magnitude of the predicted maximum principal stress is changed by dispersions about the nominal

Table 1
Nominal UHTC material properties used in analysis.[12,43,52].

Property	Value
Density (kg/m^3)	9520
CTE (K^{-1})	5.96×10^{-6}
Specific heat (J/(kg K))	270 (295 K) to 500 (2000 K)
Thermal conductivity (W/(m K))	130 (295 K) to 71 (2000 K)
Tensile modulus (GPa)	530 (295 K) to 180 (2000 K)
Poisson's ratio	0.14
Emissivity	0.9

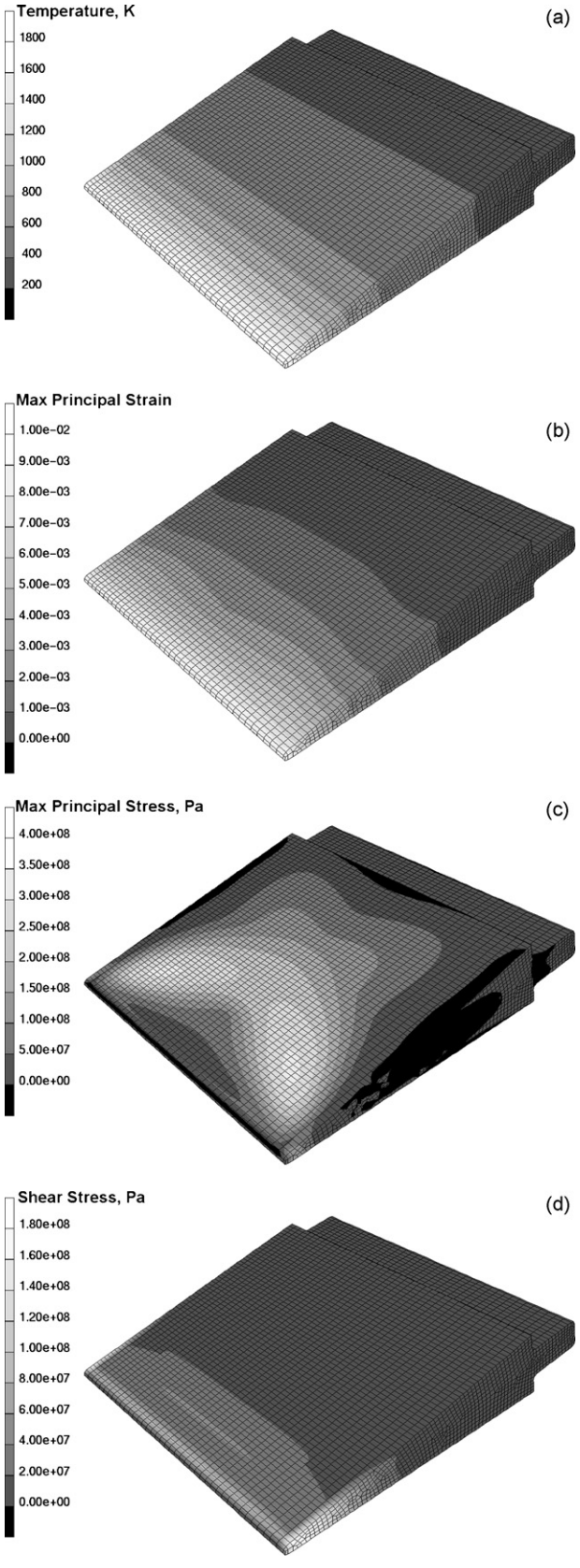

Fig. 7. Contours of (a) temperature, (b) principal total strain maxima, (c) principal tensile stress maxima, and (d) shear stress maxima, at the time of peak stress during heating, about 7 s after application of the heat flux.

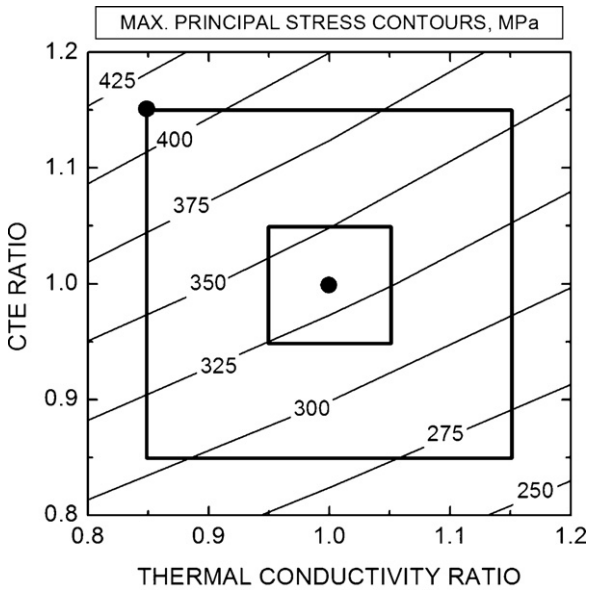

Fig. 8. Predicted maximum principal stress as a function of thermal conductivity and CTE varied about their nominal values. The center black symbol locates the maximum predicted stress (334 MPa) for the nominal property values; the inner black box is the maximum stress boundary for $\sigma = \pm 5\%$; the outer black box is the corresponding 3σ ($\pm 15\%$) boundary; the black symbol on the upper left corner of the 3σ boundary locates the maximum predicted stress (413 MPa) for the worst-case combination of property values.

thermal conductivity and CTE values. In these computations, all other material properties were held fixed. The peak tensile stress for the nominal thermal conductivity and CTE value is 334 MPa. The highest peak stresses are found for combinations of low thermal conductivity and large CTE, as expected. A standard deviation of $\sigma = \pm 5\%$ would not be unreasonable for either property, and the inner white box shows the boundaries of possible peak stress solutions for this level of uncertainty. The outer white box shows the boundaries for a corresponding 3σ analysis, as might be done by a vehicle designer. Obviously, a much larger range of possible peak stress solutions is accessed in a 3σ analysis, since the magnitude of the reported uncertainty is amplified, and it becomes much more likely that a critical maximum stress level is exceeded.

For brittle materials like UHTCs, statistical failure criteria are often associated with the volume of material stressed beyond a certain limit.[43] Fig. 9 plots the volume fractions of the UHTC WLE that exceed different levels of maximum principal tensile stress, for the nominal properties, and for the worst-case 3σ combination found in Fig. 8 (that is, a conductivity ratio of 0.85 and a CTE ratio of 1.15). The volume of WLE material in which the stress level exceeds 300 MPa increases by ~450%, going from the nominal to the worst-case combination of properties.

Note that coincident unfavorable changes in properties that have been held at nominal values in this analysis — in particular a higher tensile modulus and emissivity — could push the maximum stress magnitudes and the volume fractions exceeding certain stress levels significantly higher.

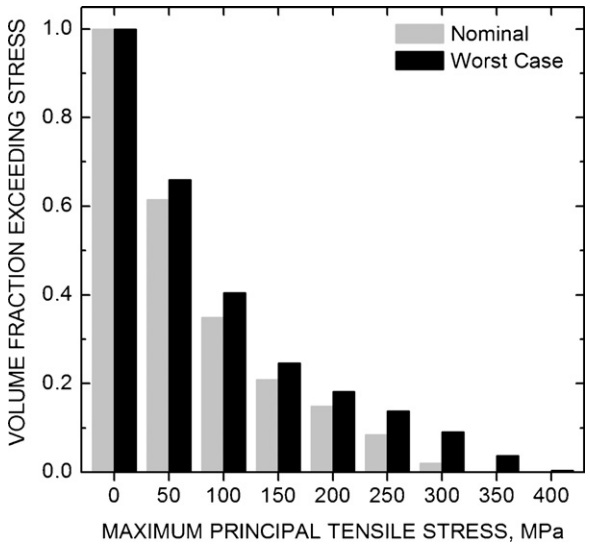

Fig. 9. The volume fraction of the UHTC WLE exceeding different levels of maximum principal tensile stress, for nominal properties and for the worst-case 3σ combination (conductivity ratio of 0.85 and CTE ratio of 1.15) in Fig. 8.

7. Conclusions

The design and analysis of UHTC components in hypersonic applications requires a complete set of accurate material properties, along with associated uncertainties and supporting information. Some key aspects that make UHTC property measurements more useful for analysts and designers are summarized below:

- The temperature dependence of material properties is always desired, but is especially critical for thermal conductivity, specific heat, emissivity, tensile modulus and thermal expansion coefficient (CTE).
- Measurement techniques should be referenced to standard tests, whenever possible.
- Measurements should always be reported with well-defined errors (that is, an explicit statement of what the error represents: technique, repeat measurements, sample-to-sample variability, and so forth).
- Isotropy and homogeneity of UHTC materials should be confirmed; failing that, the orientation of test specimens relative to the manufacturing process should be stated.

Material developers should strive to work closely with the application developers to deliver the best material property information possible. High fidelity material properties, together with well-defined uncertainties, statistically significant data sets, and supporting information, lead to more accurate performance predictions and a tighter design space.

Acknowledgments

The authors wish to thank Dr. Joan Fuller of the Air Force Office of Scientific Research (AFOSR) for suggesting the topic of this paper. The contributions of Jochen Marschall were supported by AFOSR contract FA9550-08-C-0049. Information for this paper was gathered from several NASA programs, including the Space Launch Initiative, Next Generation Launch Technology, and the Fundamental Aeronautics Program.

References

1. Upadhya K, Yang J-M, Hoffman WP. Materials for ultrahigh temperature structural applications. *Am Ceram Soc Bull* 1997;**76**:51–6.
2. Fridlender BA, Neshpor VS, Ordan'yan SS, Unrod VI. Thermal conductivity and diffusivity of binary alloys of the ZrC–ZrB_2 system at high temperature. *High Temp* 1979;**17**:1001–5.
3. Opeka MM, Talmy IG, Wuchina EJ, Zaykoski JA, Causey SJ. Mechanical, thermal, and oxidation properties of refractory hafnium and zirconium compounds. *J Eur Ceram Soc* 1999;**19**:2405–14.
4. Kolodziej P, Bowles JV, Roberts C. Optimizing hypersonic sharp body concepts from a thermal protection system perspective. In: *8th AIAA international space planes and hypersonic systems and technologies conference*. 1998.
5. Fahrenholtz WG, Hilmas GE, Talmy IG, Zaykoski JA. Refractory diborides of zirconium and hafnium. *J Am Ceram Soc* 2007;**90**:1347–64.
6. Opeka MM, Talmy IG, Zaykoski JA. Oxidation-based materials selection for 2000 °C + hypersonic aerosurfaces: theoretical considerations and historical experience. *J Mater Sci* 2004;**39**:5887–904.
7. Monteverde F, Bellosi A. Oxidation of ZrB_2-based ceramics in dry air. *J Electrochem Soc* 2003;**150**:B552–9.
8. Clougherty EV, Pober RL, Kaufman L. Synthesis of oxidation resistant metal diboride composites. *Trans Metall Soc AIME* 1968;**242**:1077–82.
9. Tripp WC, Davis HH, Graham HC. Effect of an SiC addition on the oxidation of ZrB_2. *Ceram Bull* 1973;**52**:612–6.
10. Chamberlain AL, Fahrenholtz WG, Hilmas GE, Ellerby DT. High-strength zirconium diboride-based ceramics. *J Am Ceram Soc* 2004;**87**:1170–2.
11. Monteverde F, Scatteia L. Resistance to thermal shock and to oxidation of metal diborides—SiC ceramics for aerospace application. *J Am Ceram Soc* 2007;**90**:1130–8.
12. Gasch M, Ellerby D, Irby E, Beckman S, Gusman M, Johnson S. Processing, properties, and arc jet oxidation of hafnium diboride/silicon carbide ultra high temperature ceramics. *J Mater Sci* 2004;**39**:5925–37.
13. Guo S, Kagawa Y, Nishimura T, Tanaka H. Thermal and electrical properties in hot-pressed ZrB_2–$MoSi_2$–SiC composites. *J Am Ceram Soc* 2007;**90**:2255–8.
14. Sciti D, Brach M, Bellosi A. Long-term oxidation behavior and mechanical strength degradation of a pressurelessly sintered ZrB_2–$MoSi_2$ ceramic. *Scripta Mater* 2005;**53**:1297–302.
15. Sciti D, Brach M, Bellosi A. Oxidation behavior of a pressureless sintered ZrB_2–$MoSi_2$ ceramic composite. *J Mater Res* 2005;**20**:922–30.
16. Opila E, Levine S, Lorincz J. Oxidation of ZrB_2- and HfB_2-based ultra-high temperature ceramics: effect of Ta additions. *J Mater Sci* 2004;**39**:5969–77.
17. Reuther J, Kinney D, Smith S, Kontinos D, Gage P, Saunders D. A reusable space vehicle design study exploring sharp leading edges. In: *35th AIAA thermophysics conference*. 2001.
18. Nonweiler TRF. Heat shield design for re-entry and launch. The use of conduction-assisted radiation on sharp-edged wings. *Philos Trans R Soc Lond Series A* 1999;**357**:2197–225.
19. Gülhan A, Esser B. A study on heat flux measurements in high enthalpy flows. In: *35th thermophysics conference*. 2001.
20. Smith DM, Moody H, Wanstall C, Terrazas-Salinas I. The design and use of calorimeters for characterization of high-enthalpy flows in arc-heated test facilities. In: *11th AIAA/AAAF international conference space plane and hypersonic systems and technologies*. 2002.
21. Wright MJ, Candler GV, Bose D. Data-parallel line relaxation method for the Navier–Stokes equations. *AIAA J* 1998;**36**:1603–9.
22. Cheatwood FM, Gnoffo PA. *User's manual for the Langley aerothermodynamic upwind relaxation algorithm (LAURA), NASA TM-4764*; April 1996.
23. Anon. *MSC.MARC finite element program*. Santa Ana, CA: MSC Software; 1994.

24. Chen Y-K, Milos FS, Bull JD, Squire TH. Integrated analysis tool for ultra-high temperature ceramic slender-body reentry vehicles. In: *37th AIAA aerospace sciences meeting and exhibit*. 1999.
25. Thomas DJ. *Design and analysis of UHTC leading edge attachment. NASA CR 2002-211505*; July 2002.
26. Kowalski T, Buesking K, Kolodziej P, Bull J. *A thermostructural analysis of a diboride composite leading edge. NASA TM 110407*; July 1996.
27. Kontinos DA, Gee K, Prabhu DK. Temperature constraints at the sharp leading edge of a crew transfer vehicle. In: *35th AIAA thermophysics conference*. 2001.
28. Scatteia L, Riccio A, Rufolo G, Filippis FD, Vecchio AD, Marino G. PRORA-USV SHS: ultra high temperature ceramic materials for sharp hot structures. In: *AIAA/CIRA 13th international space planes and hypersonics systems and technologies conference*. 2005.
29. Savino R, De Stefano Fumo M, Paterna D, Serpico M. Aerothermal study of UHTC-based thermal protection systems. *Aerospace Sci Technol* 2005;**9**:151–60.
30. Monti R, de Stefano Fumo M, Savino R. Thermal shielding of a reentry vehicle by ultra-high-temperature ceramic materials. *J Thermophys Heat Transf* 2006;**20**:500–6.
31. Mulville DR. *Structural design and test factors of safety for spaceflight hardware. NASA-STD-5001*; June 1996.
32. Olynick D, Loomis M, Chen Y-K, Venkatapathy E, Allen G. New TPS design strategies for planetary entry vehicle design. In: *37th aerospace sciences meeting and exhibit*. 1999.
33. Rasky DJ, Kolodziej P, Newfield ME, Laub B, Chen Y-K. Assessing factors of safety, margins of safety, and reliability of thermal protection systems. In: *36th AIAA thermophysics conference*. 2003.
34. Sherman MM. *Entry thermal protection. NASA-SP-8014*; August 1968.
35. Squire TH, Milos FS, Hartlieb GC. Aerospace materials property database (TPS*X*). *J Spacecraft Rock* 2009;**46**:733–6.
36. Chen Y-K, Squire T, Laub B, Wright M. Monte Carlo analysis for spacecraft thermal protection system design. In: *9th AIAA/ASME joint thermophysics and heat transfer conference*. 2006.
37. Cowan RD. Pulse method of measuring thermal diffusivity at high temperatures. *J Appl Phys* 1963;**34**:926–7.
38. Chamberlain AL, Fahrenholtz WG, Hilmas GE. Pressureless sintering of zirconium diboride. *J Am Ceram Soc* 2006;**89**:450–6.
39. Zhu A, Fahrenholtz WG, Hilmas GE. Influence of silicon carbide particle size on the microstructure and mechanical properties of zirconium diboride-silicon carbide ceramics. *J Eur Ceram Soc* 2007;**27**:2077–83.
40. Monteverde F. Progress in the fabrication of ultra-high-temperature ceramics: "in situ" synthesis, microstructure and properties of a reactive hot-pressed HfB_2-SiC composite. *Compos Sci Technol* 2005;**65**:1869–79.
41. Monteverde F, Bellosi A. Development and characterization of metal-diboride-based composites toughened with ultra-fine SiC particulates. *Solid State Sci* 2005;**7**:622–30.
42. Monteverde F, Guicciardi S, Bellosi A. Advances in microstructure and mechanical properties of zirconium diboride based ceramics. *Mater Sci Eng* 2003;**A346**:310–9.
43. Bull J, Kolodziej P, Salute J, Keese D. *Design, instrumentation and preflight testing of a sharp ultra-high temperature ceramic nose tip. NASA TM-1998-112229*; October 1998.
44. Marschall J, Erlich DC, Manning H, Duppler W, Ellerby D, Gasch M. Microhardness and high-velocity impact resistance of HfB_2/SiC and ZrB_2/SiC composites. *J Mater Sci* 2004;**39**:5959–68.
45. Sanders WA, Probst HB. Hardness of five borides at 1625 °C. *J Am Ceram Soc* 1966;**49**:231–2.
46. Fahrenholtz WG, Hilmas GE, Chamberlain AL, Zimmermann JW. Processing and characterization of ZrB_2-based ultra-high temperature monolithic and fibrous monolithic ceramics. *J Mater Sci* 2004;**39**:5951–7.
47. Monteverde F. Ultra-high temperature HfB_2-SiC ceramics consolidated by hot-pressing and spark plasma sintering. *J Alloys Compd* 2007;**428**:197–205.
48. Monteverde F, Bellosi A, Guicciardi S. Processing and properties of zirconium diboride-based composites. *J Eur Ceram Soc* 2002;**22**: 279–88.
49. Monteverde F, Melandri C, Guicciardi S. Microstructure and mechanical properties of an HfB_2 + 30 vol.% SiC composite consolidated by spark plasma sintering. *Mater Chem Phys* 2006;**100**:513–9.
50. Kalish D, Clougherty EV, Kreder K. Strength, fracture mode, and thermal stress resistance of HfB_2 and ZrB_2. *J Am Ceram Soc* 1969;**52**:30–6.
51. Keihn FG, Keplin EJ. High-temperature thermal expansion of certain group IV and group V diborides. *J Am Ceram Soc* 1967;**50**:81–4.
52. Gasch M, Johnson S, Marschall J. Thermal conductivity characterization of hafnium diboride-based ultra high temperature ceramics. *J Am Ceram Soc* 2008;**91**:1423–32.
53. Guo S-Q, Kagawa Y, Nishimura T, Chung D, Yang J-M. Mechanical and physical behavior of spark plasma sintered ZrC–ZrB_2–SiC composites. *J Eur Ceram Soc* 2008;**28**:1279–85.
54. Zimmermann JW, Hilmas GE, Fahrenholtz WG, Dinwiddie RB, Porter WD, Wang H. Thermophysical properties of ZrB_2 and ZrB_2–SiC ceramics. *J Am Ceram Soc* 2008;**91**:1405–11.
55. Tye RP, Clougherty EV. The thermal and electrical conductivities of some electrically conducting compounds. In: *Proceedings of the fifth symposium on thermophysical properties*. 1970. p. 396–401.
56. Wuchina E, Opeka M, Causey S, Buesking K, Spain J, Cull A, Routbort J, Guitierrez-Mora F. Designing for ultrahigh-temperature applications: the mechanical and thermal properties of HfB_2, HfC_x, HfN_x and α-Hf(N). *J Mater Sci* 2004;**39**:5939–49.
57. Wuchina E, Opeka M, Gutierrez-Mora F, Koritala RE, Goretta KC, Routbort JL. Processing and mechanical properties of materials in the Hf-N system. *J Eur Ceram Soc* 2002;**22**:2571–6.
58. Scatteia L, Borrelli R, Cosentino G, Bêche E, Sans J-L, Balat-Pichelin M. Catalytic and radiative behaviors of ZrB_2–SiC ultrahigh temperature ceramic composites. *J Spacecraft Rock* 2006;**43**:1004–12.
59. Scatteia L, Alfano D, Monteverde F, Sans J-L, Balat-Pichelin M. Effect of machining method on the catalytic and emissivity of ZrB_2 and ZrB_2–HfB_2-based ceramics. *J Am Ceram Soc* 2008.
60. Marschall J, Pejaković DA, Fahrenholtz WG, Hilmas GE, Zhu S, Ridge J, Fletcher DG, Asma CO, Thömel J. Oxidation of ZrB_2–SiC ultra-high temperature ceramic composites in dissociated air. *J Thermophys Heat Transf* 2009;**23**:267–78.
61. Monteverde F, Savino R. Stability of ultra-high temperature ZrB_2–SiC ceramics under simulated atmospheric re-entry conditions. *J Eur Ceram Soc* 2007;**27**:4797–805.
62. Marschall J, Chamberlain A, Crunkleton D, Rogers B. Catalytic atom recombination on ZrB_2/SiC and HfB_2/SiC ultrahigh-temperature ceramic composites. *J Spacecraft Rock* 2004;**41**:576–81.
63. Savino R, De Stefano Fumo M, Silvestroni L, Sciti D. Arc-jet testing on HfB_2 and HfC-based ultra-high temperature ceramic materials. *J Eur Ceram Soc* 2008;**28**:1899–907.
64. Reda DC. Correlation of nosetip boundary-layer transition data measured in ballistic-range experiments. *AIAA J* 1981;**19**:329–39.
65. Reda DC. Review and synthesis of roughness-dominated transition correlations for reentry applications. *J Spacecraft Rock* 2002;**39**: 161–7.
66. Reda DC, Wilder MC, Bogdanoff DW, Prabhu DK. Transition experiments on blunt bodies with distributed roughness in hypersonic free flight. In: *45th AIAA aerospace sciences meeting and exhibit*. 2007.
67. Kinney DJ, Bowles JV, Yang LH, Roberts CD. Conceptual design of a "SHARP"-CTV. In: *35th AIAA thermophysics conference*. 2001.